Complex exsolution microstructures in inverted pigeonites from the Sjelset Igneous Complex, Rogaland, SW Norway

J. T. KLOPROGGE, H. L. M. VAN ROERMUND & C. MAIJER

Kloprogge, J. T., van Roermund, H. L. M. & Maijer, C.: Complex exsolution microstructures in inverted pigeonites from the Sjelset Igneous Complex, Rogaland, SW Norway. *Norsk Geologisk Tidsskrift*, Vol. 69, pp. 239–249. Oslo 1989. ISSN 0029–196X.

An optical and electron microscope study has been made of inverted pigeonite from the Sjelset Igneous Complex, Rogaland, SW Norway. The inverted pigeonites reveal a Stillwater-type of microstructure: the pigeonite to orthopyroxene transformation has been pre- and post-dated by two stages of augite exsolution (parallel to $(001)_{pig}$ and $(100)_{opx}$, respectively). In addition, two distinct microstructural domains have been recognized: (1) single and (2) clusters of inverted pigeonite crystals. Most clusters of pigeonite crystals have been replaced by single orthopyroxene crystals which exhibit domains of differently oriented $(001)_{pig}$ exsolution lamellae. The mechanism of exsolution is interpreted to be heterogeneous nucleation and growth, while the transformation of pigeonite to orthopyroxene is regarded as massive.

J. T. Kloprogge, H. L. M. van Roermund and C. Maijer, Institute of Earth Sciences, Department of Petrology, State University of Utrecht, Budapestlaan 4, P.O. Box 80.021, 3508 TA Utrecht, The Netherlands. * Present address: Ecole Normale Superieure de Lyon, 46, Allée d'Italie, 69364 Lyon, Cedex 07, France.*

Due to their superior resolution, electron-optical instruments (TEM/SEM/AEM) have greatly enhanced microstructural research on natural mineral systems. One important application is the study of solid-state phase transformations. Current research has demonstrated that supersaturated solid solutions (e.g. feldspars, pyroxenes, amphiboles) produce a wide variety of exsolution microstructures during cooling. Each distinct microstructure corresponds to a particular transformation mechanism. Which mechanism was operative depends on the cooling history of the particular mineral (Shewmon 1969; McConnell 1975; Putnis & McConnell 1980; Boland 1985).

Therefore, a microstructural study of the transformation mechanisms which operated in a supersaturated solid solution allows us to reconstruct its cooling history in terms of a particular trajectory in Time–Temperature–Transformation (TTT) space.

The present paper reports on an optical, electron microscope and electron microprobe study of the subsolidus microstructural evolution of inverted pigeonite crystals from the Sjelset Igneous Complex of Rogaland, SW Norway. Two distinct microstructural types have been recognized. Each type is described and the transformation mechanism is explained.

Geological setting

The Precambrian basement of Rogaland, SW Norway, consists of two main units:

(a) The Egersund intrusive complex comprising massif-type anorthosites and the Bjerkreim–Sokndal lopolith (Duchesne & Michot 1984; Duchesne et al. 1985).
(b) A high-grade (HT/LP) metamorphic envelope with intercalated igneous complexes surrounding the Bjerkreim–Sokndal lopolith (Maijer & Padget 1987; Tobi et al. 1984; Jansen et al. 1984).

The Sjelset Igneous Complex (S.I.C.) consists of a slightly-deformed granitic body, previously mapped as 'Adamellite de Sjelset' (Michot 1960), 'Adamellite charnochitique' (Michot & Pasteels 1972) or porphyritic granite (Jorde 1980; Birkeland 1981).

The S.I.C. was emplaced into the high grade migmatite envelope, about 1020 ± 67 MA (Visser

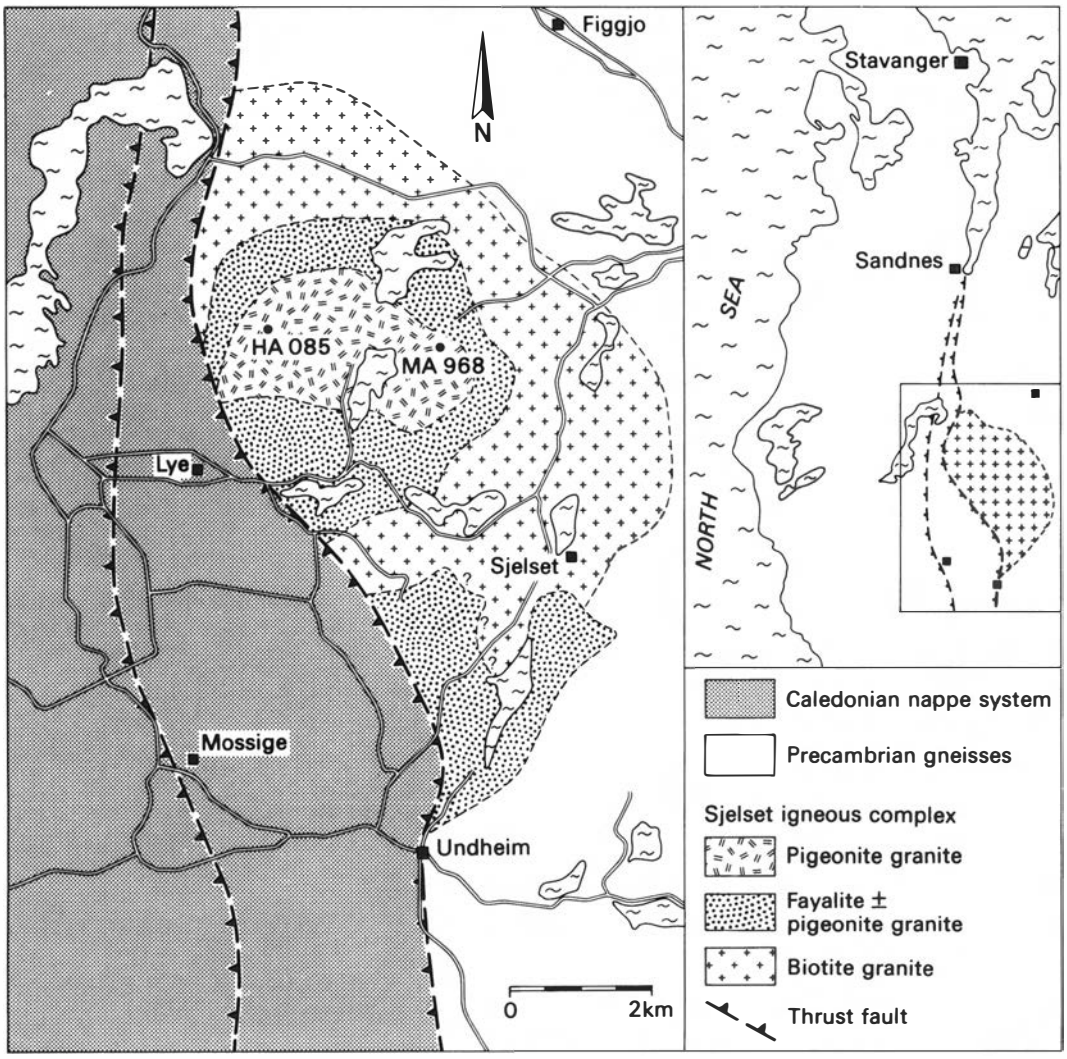

Fig. 1. Geological map of the Sjelset Igneous Complex illustrating sample localities MA968 and HA085.

et al. 1987). It is located roughly 10 km NNE of the Egersund Intrusive Complex and ca. 20 km SSE of Stavanger. On its westernmost side the S.I.C. is truncated by the Caledonian Nappe Front (Fig. 1).

The S.I.C. has been subdivided into three main rock types (Fig. 1):

(1) two feldspar–biotite granite
(2) Fe-rich, two-feldspar–pigeonite granite
(3) Fe-rich, two-feldspar–pyroxene–fayalite granites.

The coarse-grained, Fe-rich, pyroxene (± fayalite) granites also contain brown or greenish brown hornblende, ilmenite, magnetite, apatite and zircon.

All samples studied are from the Fe-rich, pyroxene granites. MA968 and HA085 (Fig. 1) have been studied in detail using optical and electron microscopy techniques.

Analytical techniques

Quantitative mineral analyses were obtained at the Institute of Earth Sciences, Utrecht, using an electron microprobe built by T.P.D., Delft, the Netherlands (operating conditions 15 kV, 0.001

μA). Furthermore, EDS was available on a JEOL 200C scanning transmission electron microscope (STEM) at the Institute of Earth Sciences, University of Utrecht, the Netherlands.

The crystallographic orientations of coarse exsolved phases and their host grains have been investigated using a 5-axis universal stage mounted on an optical microscope. Fine scale exsolution microstructures have been investigated using conventional imaging and diffraction techniques on the JEOL 200C STEM (operated at 200 kV) at Utrecht, the Netherlands.

Petrography

MA968 and HA085 reveal a cumulate texture: fine grained (<2 mm) Fe–Mg silicates, ilmenite, magnetite, apatite and zircon fill the interstices between coarse grained (up to 1 cm) euhedral to subhedral, unzoned plagioclase (≈30 % An), microperthite and quartz. Plagioclase contains albite and sometimes Carlsbad twins. Myrmekitic intergrowths of quartz and feldspar are present at interfaces between plagioclase and K-feldspar. Orthopyroxenes contain several sets of exsolution lamellae as well as inclusions of ilmenite, magnetite, apatite and zircon. Brown-green to blue-green hornblende forms rims around opaques as well as around some orthopyroxenes. A small amount of secondary calcite can be present. Minor augite is present as subhedral to euhedral grains surrounding the orthopyroxenes. Frequently the augite is in crystallographic continuity with one of the sets of augite lamellae in orthopyroxene. For this reason augite is regarded as a secondary phase. All minerals reveal undulose extinction.

Temperature-dependent fitting of host and exsolved lattices

The cell parameters of augite and pigeonite are dependent upon temperature and composition (Prewitt et al. 1971; Turnock et al. 1973; Nakazawa & Hafner 1977). Fig. 2a shows this dependency for augite and pigeonite with a X_{Fe} (=Fe/Fe + Mg) of 0.85 using the data of Turnock et al. (1973), Ross et al. (1973) and Rietmeijer & Champness (1982). Based on Fig. 2a the misfit ratio, defined as a = a(pig)/a(aug) and c = c(pig)/c(aug), shows a non-linear relationship as a function of temperature (Fig. 2b) (Nakazawa & Hafner 1977). Fig. 2b illustrates that at elevated temperatures the $(001)_{pig}$ lamellae are the most stable configuration. As the temperature drops the misfit ratio of the $(001)_{pig}$ lamellae increases resulting in the formation of the more stable $(100)_{opx}$ lamellae at lower temperatures. Experimental work indicates that the change in orientation of the lamellae from $(001)_{pig}$ to $(100)_{opx}$ approximately coincides with the pigeonite–orthopyroxene transition (Prewitt et al. 1971;

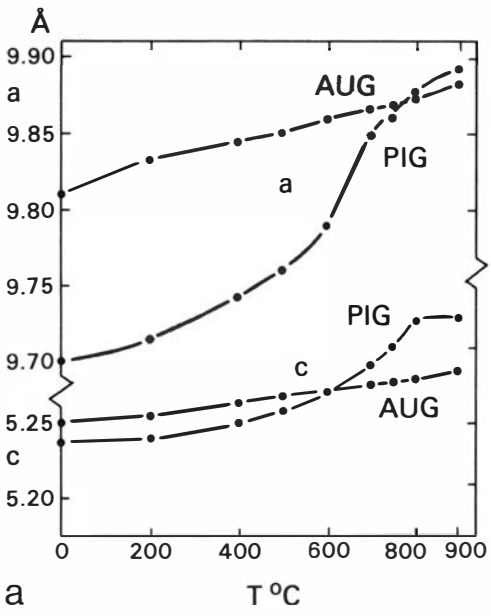

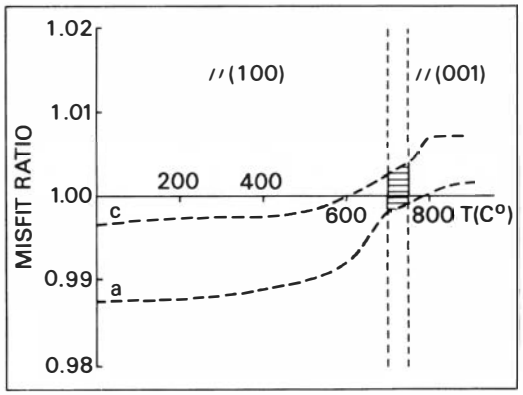

Fig. 2a. Temperature dependency of the a- and c-axes of pigeonite and augite with X_{Fe} = 0.85 (after Rietmeijer & Champness 1982). b. Temperature dependency of the misfit ratio based on Fig. 2a indicating a change of lamella orientation at 700–750°C.

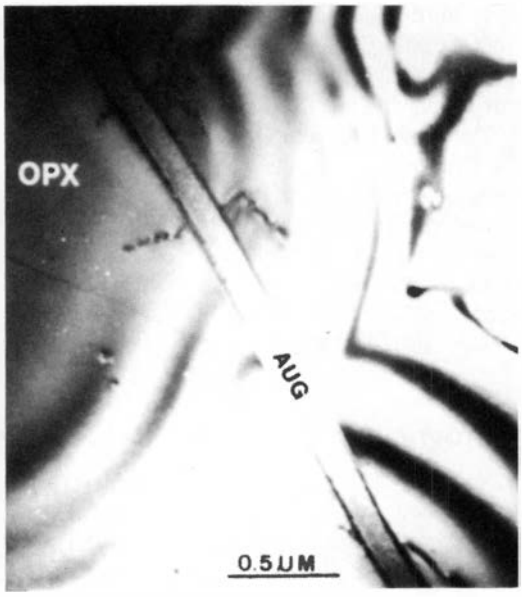

*Fig. 3*a. Coarse $(001)_{pig}$ exsolution microstructure. b. Fine $(001)_{pig}$ lamellae. c. Coarse and fine $(100)_{opx}$ lamellae.

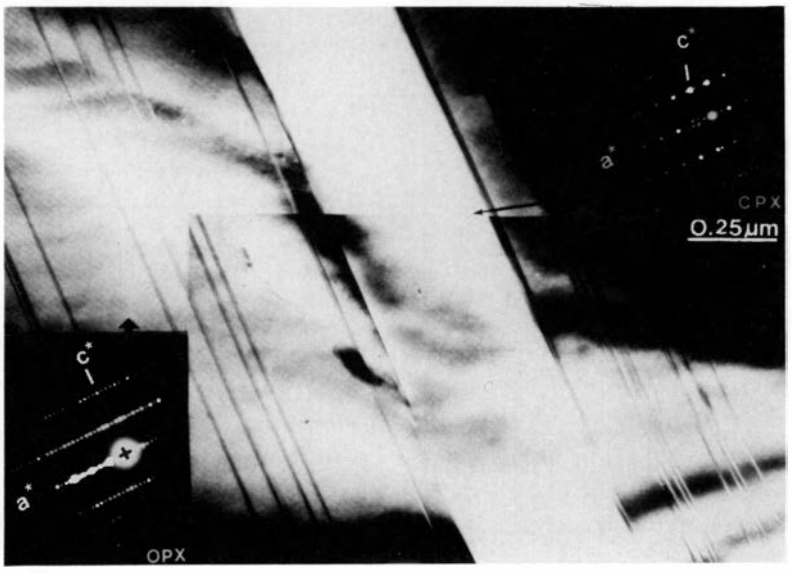

Nakazawa & Hafner 1977). From Fig. 2b it is concluded that this change in orientation of the lamellae takes place approximately between 700° and 750°C.

Inverted pigeonite morphology

Within the interstices of the cumulate, the inverted pigeonite reveals a 'Stillwater type' of

exsolution microstructure (Takeda 1973; Ishii & Takeda 1974; Rietmeijer 1979; Ranson 1986) in which the orthopyroxene is characterized by two generations of exsolved augite lamellae approximately parallel to the original $(001)_{pig}$ plane (Fig. 3a, b).

Excess Ca is exsolved after inversion, again in two stages, as augite lamellae parallel to $(100)_{opx}$ (Fig. 3c). Using optical and EM techniques, Fe–Ti exsolution microstructures have been recognized within the individual exsolved augite lamellae.

Coarse $(001)_{pig}$ augite lamellae range in size from 20 to 100 μm. Locally they also occur as blebs or irregular domains (Fig. 3a). Fine scale $(001)_{pig}$ augite lamellae can only be resolved using TEM techniques. Their thickness is about 0.25 μm. Coarse $(100)_{opx}$ lamellae range in thickness from 0.3 to 0.5 μm and are optically visible in some thin sections. Small $(100)_{opx}$ lamellae are only 2–3 unit cells thick (Fig. 3c), and consequently they can only be resolved by TEM.

Interfaces between inverted pigeonites and coarse and fine $(001)_{pig}$ lamellae are almost always non-coherent and irrational (but see Fig. 4c, 1). In

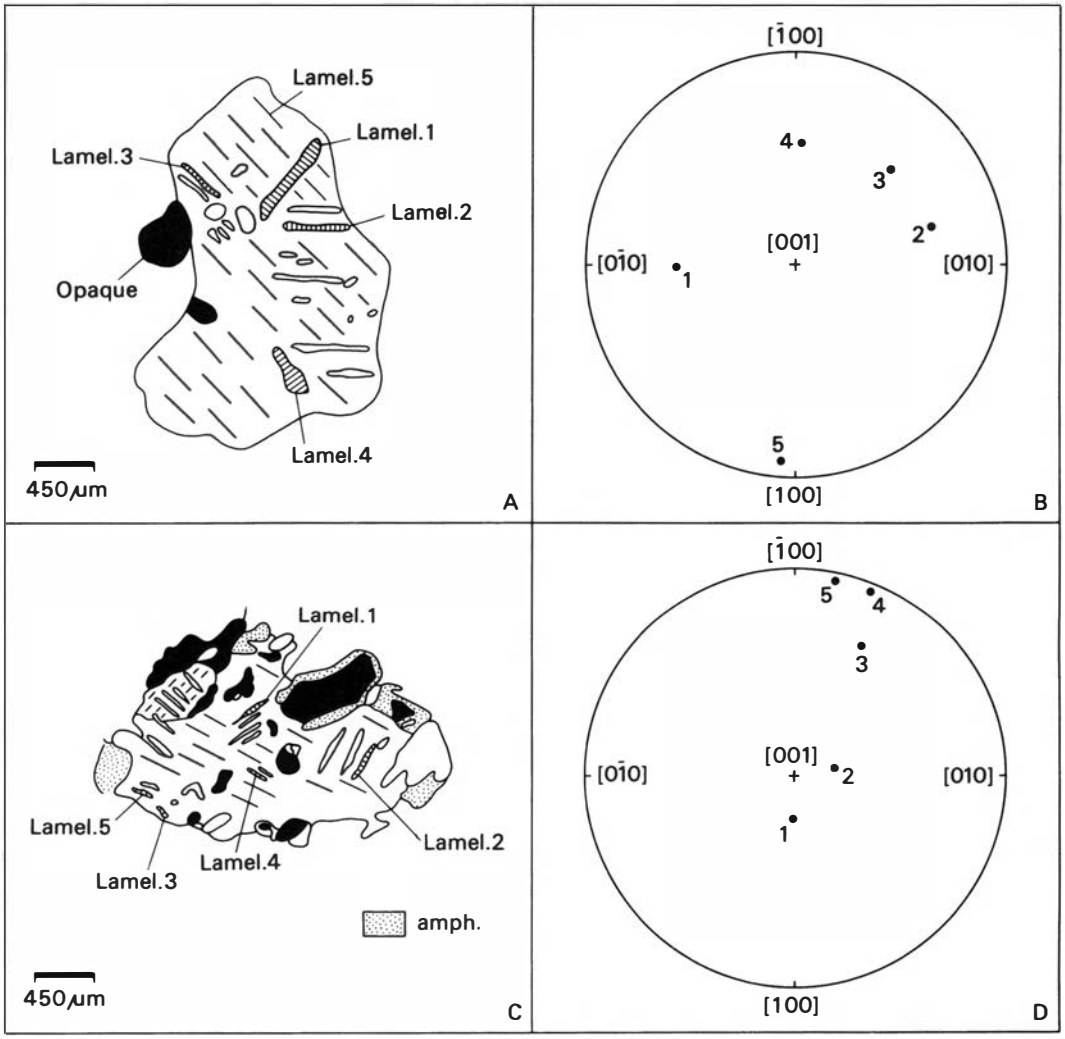

Fig. 4. Optical data on interface morphology of coarse $(001)_{pig}$ lamellae. The plots in B and D give the orientation of the lamella interfaces, plotted as normals of the interfacial planes, with respect to the orthopyroxene crystallographic orientation for A and C, respectively.

contrast, interfaces between inverted pigeonites and coarse and fine $(100)_{opx}$ lamellae are always coherent and rational (parallel to $(100)_{opx}$, Figs. 4a, 5). In addition, a few isolated ledges (0.007 μm thick) characterize the interface between orthopyroxene and coarse $(100)_{opx}$ lamellae.

Among the inverted pigeonite crystals two types of microstructures can be distinguished: (1) isolated single crystals of inverted pigeonite with Stillwater type of exsolution microstructures; (2) inverted pigeonites comprising several original pigeonite crystals. Prior to the transformation of pigeonite to orthopyroxene, exsolution of augite lamellae approximately parallel to $(001)_{pig}$ took place. These $(001)_{pig}$ augite lamellae can now be recognized as domains of parallel augite lamellae within one single orthopyroxene host (Fig. 3a). Consequently, when the orientation of the crystallographic axes of the $(001)_{pig}$ augite lamellae is compared with that of the orthopyroxene host, most lamellae appear to be unrelated (Fig. 5). Sometimes, however, close inspection reveals one set of augite lamellae to be related to the crystallographic axes of the host grain, for example Fig. 5a, 1. Subsequent exsolution of $(100)_{opx}$ augite lamellae took place throughout the entire orthopyroxene host. Universal-stage measurements between coarse $(001)_{pig}$ lamellae and inverted pigeonites in the isolated single crystal also show no crystallographic continuity between the orthopyroxene host and the exsolved $(001)_{pig}$ lamellae.

EMP analyses

Electron microprobe (EMP) analyses of coarse $(001)_{pig}$ augite lamellae and their host orthopyroxene are presented in Table 1. The local scatter in Ca content in orthopyroxene is interpreted to be due to incorporation of submicroscopic $(100)_{opx}$ augite lamellae. Furthermore, Ca in inverted pigeonites is generally lower than within pigeonite. For clinopyroxene lamellae the Ca enrichment is apparent as well as a reduction of the Fe/Mg

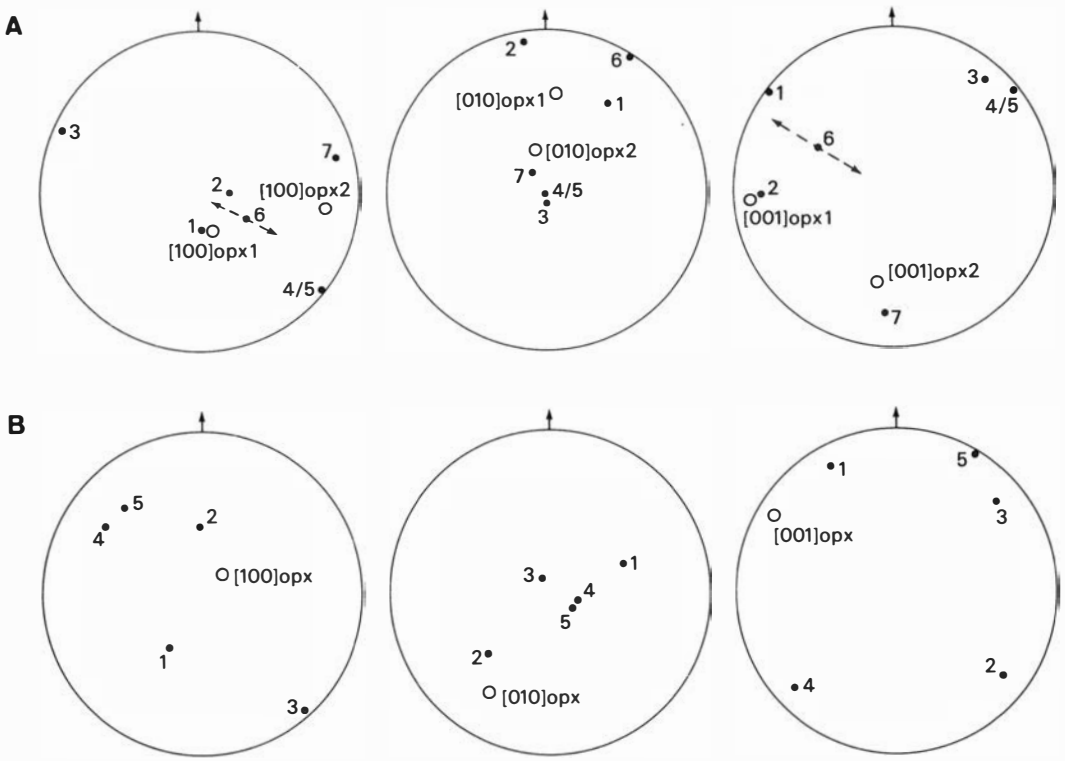

Fig. 5. Optical data on the crystallographic relationship between coarse $(001)_{pig}$ lamellae and the orthopyroxene host. The orientations of the normals of the planes [100], [010] and [001] of the lamellae with respect to [100], [010] and [001] of the orthopyroxene host are given. A. Inverted pigeonite crystal from Fig. 3a. B. Inverted pigeonite crystal from Fig. 4c.

ratio. All EMP analyses reveal a low content of Cr, Ti, Mn and Na.

EMP analyses of pairs of inverted pigeonites and coarse $(001)_{pig}$ augite lamellae have been used to estimate the closing temperature of the Mg, Fe, Ca exchange between the coexisting phases using the methods given by Wood & Banno (1973), Wells (1977) and Lindsley & Andersen (1983). Equilibrium temperatures according to Wood & Banno are 800 ± 90°C and Wells 845 ± 120°C. Temperatures obtained using Lindsley & Andersen's thermometer show a wide scatter ranging from 900°C to 500°C. Ranson (1986) mentioned the same problem in a few of his samples. We regard Lindsley & Andersen's thermometer as being unrealistic in this case. The Mg, Fe, Ca exchange blocking temperatures for the pigeonites have been estimated using Ishii's (1975) thermometer. Results indicate temperatures of around 890°C (±50°C).

Semi-quantitative analyses using EDS on the JEOL 200C confirmed that the fine-scale $(001)_{pig}$ and coarse-scale $(100)_{opx}$ lamellae in inverted pigeonites are augite.

Discussion

Heterogeneous nucleation on grain boundaries and linear defects is generally accepted to be the nucleation mechanism involved in the formation of the various $(001)_{pig}$ and $(100)_{opx}$ augite precipitates (Champness & Lorimer 1978; Putnis & McConnell 1980). Subsequent growth of the precipitates takes place by the migration of ledges.

However, three different transformation mechanisms have recently been proposed for the polymorphic phase transition of pigeonite to orthopyroxene (Buseck et al. 1980). Fundamental in the classification scheme for the pigeonite to orthopyroxene transformation mechanism is the relationship between the orientation of the crystallographic axes of the pigeonite parent and orthopyroxene product. In the case where crystallographic continuity is retained between parent and product the transformation is generally accepted to be produced by a martensitic transformation which takes place by glide on (100) using partial dislocations with Burgers vector 0.83 [001] (Coe & Kirby 1975).

In cases where there is a lack of a common crystallographic orientation between the pigeonite parent and orthopyroxene product the transformation mechanism is interpreted to be either massive, or eutectoidal decomposition (Champness & Copley 1976; Buseck et al. 1980; Boland 1985). Massive transformations are diffusionless, 'civilian' transformations for which nucleation occurs preferentially at grain boundaries and growth proceeds by the rapid propagation of an incoherent interface, disregarding pre-existing grain boundaries (Massalski 1970). This mechanism has been proposed by Champness & Copley (1976) and Rietmeijer (1979) to explain inverted pigeonite microstructures in which the original pigeonite crystallographic axes had been disregarded during the transformation, but each new orthopyroxene crystal had encompassed several pre-existing pigeonite grains.

The typical microstructure that is produced during discontinuous precipitation reactions (eutectoidal and spinodal decomposition) is the formation of a duplex structure which is the product of the reaction that proceeds via the simultaneous migration of the boundary and growth of the decomposed phase(s) after the product phases have been nucleated heterogeneously along the grain boundary. In general, crystallographic continuity remains between one of the product phases (orthopyroxene) and a parent grain (pigeonite) on one side of the grain boundary. Also due to reduction of the interfacial energy there is a consistent crystallographic relationship between both phases in the duplex structure. Although the duplex structure might have been modified during later-stage coarsening processes the duplex microstructure is crucial in identifying this transformation mechanism.

Inverted pigeonites with blebby augite sharing (100) with the host orthopyroxene have been interpreted to be produced by the discontinuous reaction mechanism (Ishii & Takeda 1974).

The relative positions of the martensitic, massive and discontinuous reaction curves in time–temperature–transformation (T–T–T) space are unknown for pigeonite compositions, but in alloys the massive transformation usually occurs at a higher temperature (slower cooling rate) than the martensitic one, while discontinuous reactions take place at higher temperatures (slower cooling rate) than massive transformations.

From the discussion above it is concluded that the two types of inverted pigeonite microstructures that are present in the Sjelset Igneous Complex are the result of a massive phase transformation.

Table 1. Representative EMP analyses of MA968 and HA085.

MA968 pigeonite granite, inverted pigeonite										
SiO_2	47.03	46.93	46.69	46.68	45.95	45.98	47.82	46.95	47.40	46.59
Al_2O_3	0.68	0.46	0.41	0.62	0.62	0.43	0.52	0.56	0.68	0.54
Cr_2O_3	0.00	0.00	0.00	0.00	0.07	0.00	0.00	0.10	0.00	0.00
TiO_2	0.17	0.00	0.10	0.00	0.11	0.21	0.00	0.11	0.00	0.00
FeO	41.47	46.94	47.44	47.81	44.67	44.45	43.18	45.20	44.71	39.52
MnO	0.79	0.96	0.80	0.81	0.66	0.90	0.72	0.80	0.69	0.53
MgO	4.09	4.48	4.15	4.28	4.44	4.29	4.41	4.24	4.50	4.06
CaO	6.01	0.90	1.24	0.93	2.36	3.08	4.60	2.48	3.19	7.38
Na_2O	0.28	0.30	0.30	0.00	0.16	0.00	0.30	0.00	0.33	0.00
tot.	100.52	100.97	101.13	101.13	99.04	99.34	101.55	100.44	101.50	98.62
Si	1.950	1.960	1.951	1.956	1.950	1.950	1.966	1.971	1.955	1.968
Al	0.034	0.023	0.021	0.031	0.031	0.022	0.026	0.028	0.033	0.027
Cr	0.000	0.000	0.000	0.000	0.003	0.000	0.000	0.004	0.000	0.000
Ti	0.006	0.000	0.003	0.000	0.004	0.007	0.000	0.004	0.000	0.000
Fe^{3+}	0.078	0.076	0.090	0.054	0.072	0.064	0.064	0.016	0.082	0.038
Fe^{2+}	1.361	1.564	1.568	1.621	1.513	1.512	1.421	1.571	1.460	1.357
Mn	0.028	0.034	0.029	0.029	0.024	0.033	0.026	0.029	0.025	0.019
Mg	0.252	0.279	0.259	0.268	0.281	0.272	0.271	0.266	0.277	0.256
Ca	0.267	0.041	0.056	0.042	0.107	0.140	0.203	0.112	0.141	0.334
Na	0.023	0.025	0.025	0.000	0.014	0.000	0.024	0.000	0.027	0.000
sum	3.999	4.002	4.002	4.001	3.999	4.000	4.001	4.001	4.000	3.999
X_{Fe}	0.851	0.855	0.865	0.862	0.849	0.853	0.846	0.856	0.848	0.845
MA968, coarse clinopyroxene lamellae										
SiO_2	48.51	48.85	47.52	47.53	47.39	47.90	49.17	48.43	47.78	49.05
Al_2O_3	1.00	0.99	0.99	1.14	1.28	0.91	0.98	0.98	1.56	1.09
Cr_2O_3	0.00	0.00	0.00	0.08	0.00	0.00	0.00	0.00	0.00	0.00
TiO_2	0.15	0.13	0.20	0.18	0.19	0.16	0.13	0.11	0.11	0.17
FeO	25.04	25.77	24.86	25.26	28.48	24.71	24.93	25.53	29.31	27.36
MnO	0.26	0.39	0.25	0.36	0.44	0.38	0.33	0.50	0.36	0.47
MgO	3.99	4.18	4.08	3.95	3.94	3.71	3.88	3.75	4.12	3.95
CaO	20.85	19.11	20.71	19.74	16.90	20.58	20.75	20.20	15.55	19.14
Na_2O	0.58	0.68	0.37	0.40	0.18	0.33	0.15	0.00	0.15	0.27
tot.	100.38	100.10	98.98	98.64	98.80	98.68	100.32	99.50	98.94	101.50

Si	1.933	1.953	1.923	1.933	1.943	1.949	1.969	1.963	1.958	1.949
Al	0.048	0.047	0.048	0.055	0.062	0.044	0.047	0.047	0.076	0.052
Cr	0.000	0.000	0.000	0.003	0.000	0.000	0.000	0.000	0.000	0.000
Ti	0.005	0.004	0.006	0.006	0.006	0.005	0.004	0.004	0.003	0.005
Fe^{3+}	0.116	0.092	0.122	0.090	0.054	0.072	0.018	0.018	0.012	0.058
Fe^{2+}	0.718	0.769	0.719	0.769	0.922	0.769	0.817	0.847	0.992	0.851
Mn	0.009	0.013	0.009	0.013	0.015	0.013	0.011	0.017	0.013	0.016
Mg	0.237	0.249	0.246	0.240	0.241	0.226	0.232	0.227	0.252	0.234
Ca	0.891	0.819	0.898	0.861	0.742	0.897	0.890	0.877	0.683	0.815
Na	0.046	0.053	0.030	0.032	0.015	0.026	0.012	0.000	0.012	0.022
sum	4.003	3.999	4.001	4.002	4.000	4.001	4.000	4.000	4.001	4.002
X_{po}	0.779	0.776	0.774	0.782	0.802	0.788	0.783	0.792	0.799	0.795

HAO85, pigeonite granite, inverted pigeonite

SiO_2	46.68	47.07	46.87	47.07	47.39	47.07	47.57	46.59	47.78	47.40
Al_2O_3	0.65	0.61	0.41	0.69	0.74	0.61	0.56	0.37	0.72	0.54
Cr_2O_3	0.08	0.00	0.14	0.00	0.00	0.00	0.00	0.00	0.00	0.00
TiO_2	0.15	0.07	0.07	0.13	0.00	0.00	0.07	0.07	0.00	0.00
FeO	45.70	45.20	45.77	43.80	43.09	45.09	42.68	43.03	42.43	42.40
MnO	0.85	0.79	1.00	0.87	0.73	0.65	0.70	0.79	0.70	0.76
MgO	4.32	4.40	4.22	4.20	4.27	4.20	4.25	4.50	4.44	4.31
CaO	1.32	1.80	1.15	3.57	3.79	2.15	4.01	2.99	4.26	4.48
Na_2O	0.34	0.60	0.39	0.00	0.22	0.00	0.19	0.34	0.19	0.18
tot.	100.09	100.54	100.02	100.33	100.23	99.77	100.03	98.68	100.52	100.07
Si	1.964	1.961	1.974	1.973	1.978	1.988	1.991	1.975	1.985	1.981
Al	0.032	0.030	0.020	0.033	0.037	0.031	0.028	0.019	0.035	0.027
Cr	0.003	0.000	0.005	0.000	0.000	0.000	0.000	0.000	0.000	0.000
Ti	0.005	0.002	0.002	0.004	0.000	0.000	0.002	0.003	0.000	0.000
Fe^{3+}	0.051	0.095	0.060	0.013	0.024	0.000	0.000	0.052	0.009	0.024
Fe^{2+}	1.557	1.480	1.553	1.522	1.481	1.953	1.494	1.474	1.465	1.458
Mn	0.031	0.028	0.036	0.031	0.026	0.023	0.025	0.029	0.025	0.027
Mg	0.271	0.274	0.265	0.263	0.266	0.265	0.265	0.285	0.276	0.268
Ca	0.060	0.080	0.053	0.161	0.170	0.097	0.180	0.135	0.190	0.201
Na	0.028	0.049	0.033	0.000	0.019	0.000	0.016	0.029	0.016	0.015
sum	4.002	3.999	4.001	4.000	4.000	3.997	4.001	4.001	4.001	4.001
X_{Fe}	0.856	0.852	0.859	0.854	0.850	0.881	0.849	0.843	0.842	0.847

Table 1. (continued)

HA085, coarse clinopyroxene lamellae										
SiO_2	48.82	49.12	48.63	48.79	48.36	48.21	48.39	48.06	48.18	47.74
Al_2O_3	0.00	1.09	1.23	1.14	1.03	0.86	0.72	1.01	1.12	0.71
Cr_2O_3	0.00	0.00	0.00	0.00	0.00	0.12	0.00	0.00	0.00	0.00
TiO	0.00	0.21	0.26	0.43	0.12	0.19	0.41	0.22	0.27	0.12
FeO	26.03	28.60	27.01	25.50	24.33	26.01	31.81	26.25	29.10	36.99
MnO	0.56	0.37	0.44	0.57	0.53	0.55	0.55	0.45	0.55	0.87
MgO	3.80	4.06	3.87	3.76	4.11	3.84	3.91	3.93	4.20	3.91
CaO	19.21	17.01	18.08	19.13	20.10	18.80	13.79	18.97	16.66	9.05
Na_2O	0.00	0.68	0.50	0.49	0.35	0.37	0.00	0.28	0.47	0.00
tot.	98.42	101.14	100.02	99.81	98.93	98.95	99.58	99.17	100.55	99.39
Si	2.004	1.957	1.957	1.964	1.958	1.962	1.984	1.952	1.936	1.987
Al	0.000	0.052	0.059	0.054	0.050	0.042	0.035	0.049	0.054	0.035
Cr	0.000	0.000	0.000	0.000	0.000	0.004	0.000	0.000	0.000	0.000
Ti	0.000	0.007	0.008	0.013	0.004	0.006	0.013	0.007	0.008	0.004
Fe^{3+}	0.000	0.069	0.052	0.031	0.052	0.046	0.000	0.053	0.092	0.000
Fe^{2+}	0.894	0.884	0.857	0.828	0.771	0.839	1.091	0.839	0.886	1.288
Mn	0.020	0.013	0.015	0.020	0.018	0.019	0.019	0.016	0.019	0.031
Mg	0.233	0.241	0.232	0.226	0.248	0.233	0.239	0.238	0.252	0.243
Ca	0.845	0.726	0.780	0.825	0.872	0.820	0.606	0.825	0.717	0.404
Na	0.000	0.053	0.039	0.039	0.028	0.030	0.000	0.022	0.038	0.000
sum	3.996	4.002	3.999	4.000	4.001	4.001	3.986	4.001	4.002	3.991
X_{Fe}	0.793	0.798	0.797	0.792	0.768	0.792	0.820	0.789	0.795	0.841

Acknowledgements. – The establishment of the electron microscopy facility of the University of Utrecht is financed by N.W.O.-W.A.C.O.M. (Netherlands Organization for the Advancement of Pure Research). Dr. R. O. Felius is acknowledged for assistance and useful discussions.

Manuscript received June 1989

References

Birkeland, T. 1981: The geology of the Jaeren and adjacent districts. A contribution to the Caledonian Nappe Tectonics of Rogaland, Southwestern Norway. *Norsk Geologisk Tidsskrift 61*, 213–235.

Boland, J. N. 1985: Mechanisms of phase transformations in minerals. *In* White, J. C. (ed.): *M.A.C. Short Course in Applications of Electron Microscopy*, 91–120. Fredericton.

Buseck, P. R., Nord, G. L. & Veblen, D. R. 1980: Subsolidus phenomena in pyroxenes. *In* Prewitt, C. T. (ed.): *Reviews in Mineralogy, vol. 7*, 117–211. Pyroxenes; Book Crafters Inc., Chelsea, Michigan 48118.

Champness, P. E. & Copley, P. A. 1976: The transformation of pigeonite to orthopyroxene. *In* Wenk, H.-R. (ed.): *Elecron Microscopy in Mineralogy*, 228–234. Springer Verlag, Berlin.

Champness, P. E. & Lorimer, G. W. 1976: Exsolution in silicates. *In* Wenk, H.-R. (ed.): *Electron Microscopy in Mineralogy*, 174–204. Springer Verlag, Berlin.

Coe, R. S. & Kirby, S. H. 1975: The orthoenstatite to clinoenstatite transformation by shearing and reversion by annealing: mechanism and potential applications. *Contributions to Mineralogy and Petrology 52*, 29–56.

Duchesne, J., Maquil, R. & Demaiffe, D. 1985: The Rogaland anorthosites: facts and speculations. *In* Tobi, A. C. & Touret, J. L. R. (eds.): The Deep Proterozoic Crust in the North Atlantic Provinces. *NATO ASI series, serie C, vol. 158*, 449–476.

Duchesne, J. & Michot, J. 1984: The Rogaland Intrusive Masses: Introduction. *In* Maijer, C. (ed.): *Excursion Guide of the South Norway Geological Excursion*, 77–83.

Ishii, T. 1975: The relation between temperature and composition of pigeonite in some lavas and their application to geothermometry. *Mineralogical Journal 8*, 48–57.

Ishii, T. & Takeda, H. 1974: Inversion, decomposition and exsolution phenomena of terrestrial and extra-terrestrial pigeonites. *Memoires of the Geological Society of Japan 11*, 19–36.

Jansen, J. B. H., Blok, R. J. P., Bos, A. & Scheelings, M. 1984: Geothermometry and geobarometry in Rogaland and preliminary results from the Bamble Area, South Norway. *In* Tobi, A. C. & Touret, J. L. R. (eds.): The Deep Proterozoic Crust in the North Atlantic Provinces, *NATO ASI series, serie C. vol. 158*, 499–516.

Jorde, K. 1980: Geologisk Kart over Norge – 1:250000. Stavanger. NO 31-6. *Norges geologiske undersøkelse*, Trondheim.

Lindsley, D. H. & Andersen, D. J. 1983: A two pyroxene thermometer. Proceedings of the Thirteenth Lunar and Planetary Science Conference, part 2, *Journal of Geophysical Research 88*, supplement, A887–A906.

Maijer, C. & Padget, P. 1987: The geology of southernmost Norway, an excursion guide. *Norge Geologiske Undersøkelse Special Publication no. 1*. 109 pp.

Massalski, T. B. 1970: Massive transformations. *In* Chapman & Hall (eds.): Phase transformations. *American Society for Metals (Metals Park)*, 433–487. Ohio, London.

McConnell, J. D. C. 1975: Microstructures of minerals as petrogenetic indicators. *Annual Review of Earth and Planetary Sciences 3*, 129–155.

Michot, P. 1960: La Geologie de la Catazone: le Probleme des anorthosites, la Palingenese basique et la Tectonique catazonale dans le Rogaland meridional (Norvege meridional). *Excursionguide A 9 of the International Geological Congress, XXIth Session, Norden.*

Michot, J. & Pasteels, P. 1972: Aperçu Petrologique et Geochronologique sur le Complexe eruptif du Rogaland meridional et sa Couverture metamorphique. *Science de la Terre, XVIII*, 195–219.

Nakazawa, H. & Hafner, S. S. 1977: Orientation relationships of augite exsolution lamellae in pigeonite hosts. *American Mineralogist 62*, 79–88.

Prewitt, C. T., Brown, G. E. & Papike, J. J. 1971: Apollo 12 clinopyroxenes: high temperature X-ray diffraction studies. Proceedings of the 2nd Lunar Science Conference. *Geochim Cosmochim Acta supplement 2, 1*, 59–68.

Putnis, A. & McConnell, J. D. C. 1980: *Principles of Mineral Behavior*, 257 pp. Blackwell, Oxford.

Ranson, W. A. 1986: Complex exsolution in inverted pigeonite: exsolution mechanisms and temperatures of crystallization and exsolution. *American Mineralogist 71*, 1322–1336.

Rietmeijer, F. J. M. 1979: Pyroxenes from iron-rich igneous rocks in Rogaland, SW Norway. Ph.D. thesis, University of Utrecht, The Netherlands. *Geologica Ultraiectina 21*, 341 pp.

Rietmeijer, F. J. M. & Champness, P. E. 1982: Exsolution structures in calcic pyroxenes from the Bjerkreim–Sokndal lopolith, SW Norway. *Mineralogical Magazine 45*, 11–24.

Ross, M., Huebner, J. S. & Dowty, E. 1973: Delineation of the one atmosphere augite–pigeonite miscibility gap for pyroxenes from lunar basalt 12021. *American Mineralogist 58*, 619–635.

Shewmon, P. G. 1969: *Transformations in Metals*, 394 pp. McGraw-Hill, New York.

Takeda, H. 1973: Inverted pigeonites from a clast of rock 15459 and basaltic achondrites. *Proceedings of the 4th Lunar Science Conference 1*, 875–885.

Tobi, A. C., Hermans, G. A. E. M., Maijer, C. & Jansen, J. B. H. 1984: Metamorphic zoning in the high-grade proterozoic of Rogaland–Vest Agder, SW Norway. *In* Tobi, A. C. & Touret, J. L. R. (eds.): The Deep Proterozoic Crust in the North Atlantic Provinces. *NATO ASI series, serie C, vol. 158*, 477–498.

Turnock, A. C., Lindsley, D. H. & Grover, J. E. 1973: Synthesis and unit cell parameters of Ca–Mg–Fe pyroxenes. *American Mineralogist 58*, 50–59.

Visser, D., Maijer, C. & Verschure, R. H. 1987: Rb–Sr dating of the Sjelset Igneous Complex, Rogaland, Southwestern Norway. Unpublished Ms.C. thesis, University of Utrecht, Utrecht, The Netherlands.

Wells, P. R. A. 1977: Pyroxene thermometry in simple and complex systems. *Contributions to Mineralogy and Petrology 62*, 129–139.

Wood, B. J. & Banno, S. 1973: Garnet–orthopyroxene and orthopyroxene–clinopyroxene relationships in simple and complex systems. *Contributions to Mineralogy and Petrology 42*, 109–124.